# Fatigue crack initiation and propagation of 100Cr6 steel under torsional loading in very high cycle regime

*Hongqian* Xue[1,*], *Tao* Gao[1], *Zhidan* Sun[2], and *Xianjie* Zhang[1]

[1] Key Laboratory of Contemporary Design & Integrated Manufacturing Technology of Ministry of Education, Northwestern Polytechnical University, 710072, Xi'an, China
[2] ICD, P2MN, LASMIS, University of Technology of Troyes, UMR 6281, CNRS, Troyes, France

**Abstract.** Cyclic torsional fatigue properties of a high strength steel 100Cr6 are investigated using an ultrasonic torsional fatigue testing machine, and the results are compared with those obtained with fatigue tests under axial loading. Fatigue crack initiation and growth under torsion loading are observed in the very high cycle regime. Results show that fatigue cracks initiated from specimen surface as well as subsurface inclusions under torsion loading. However, subsurface MnS inclusions play a dominant role in crack initiation under torsion loading in the very high cycle regime. The initiation and early propagation of fatigue cracks are mostly controlled by the direction of the maximum shear stress. For surface crack initiation, cracks initiated in parallel to the longitudinal direction of the specimens. Once the shear crack propagated to a crack length of about 20-30 μm, crack branched to the angle close to the direction perpendicular to the remote maximum principal stresses. As for the subsurface fatigue crack initiation, the cracks parallel to the longitudinal direction of the specimens could not be observed, and crack propagation followed a spiral shape on a plane with an orientation of 45º with respect to the loading direction, which corresponds to the maximum principal stress plane.

## 1. Introduction

Structural components subjected to high frequency vibrations, such as those used in rotary parts in engines, are usually required to be designed using a lifetime failure-free criterion or an endurance limit for a very large number of cycles. Fatigue data obtained under uniaxial loading are not sufficient to assess very high cycle fatigue limit of mechanical components which are subjected to torsion loading over a wide range of cyclic frequency. In the rotary components such as transmission shafts, bearing structural components, fatigue failure occurs under the effect of combined bending and torsional loadings often at very high frequency. It is thus necessary to investigate the torsion fatigue performance of materials in very high cycle regime in order to appropriately design mechanical parts with respect to the life in service.

100Cr6 steel is a high strength steel usually used to build engine components in automotive industry. In service, the components are subjected to low amplitude, high frequency cyclic loading due to for example vehicle vibrations, and the number of cycles to failure is in the very high cycle regime. In the literature, several investigations of this steel under very high cycle fatigue have been reported. For example, Spriestersbach [1] studied the crack initiation mechanisms and threshold values of very high cycle fatigue failure for 100Cr6 steel. In reference [2], gigacycle fatigue tests were performed for 100Cr6 steel and prediction of fatigue failure was realized using a model based on the geometrical properties of inclusions. Mayer et al. [3] studied the very high cycle fatigue properties of a bainitic 100Cr6 steel, and in this work a special attention was paid to the crack initiation sites. However, most the ultrasonic fatigue tests conducted in these work are of uniaxial nature, and cyclic shear fatigue behavior and fatigue data of high strength steels in torsion are still limited in the literature. Yoshinobu [4] performed cyclic torsion fatigue test of a carburized alloy steel in very high cycle regime. They reported that crack deflection from mode II to mode I occurs under torsional loading. Akiniwa [5] also examined crack initiation and growth of several steels in the very high cycle regime. Similar to crack initiation and growth mechanisms observed for these steels, cracks initiation either perpendicular or parallel to the longitudinal direction of the specimen surface was reported under cyclic torsion loading. Recently, Mayer [6] performed ultra-high cycle torsion fatigue tests of a VDSiCr spring steel processed by shot peening at different load ratios. In this work, the interesting subsurface crack initiation has been observed under

* Corresponding author: xuedang@nwpu.edu.cn

© The Authors, published by EDP Sciences. This is an open access article distributed under the terms of the Creative Commons Attribution License 4.0 (http://creativecommons.org/licenses/by/4.0/).

torsional loading in spite of the maximum shear stress acting at the specimen. They pointed out that subsurface crack initiation occurs due to the effect of surface residual compression stress of specimen processed by shot peening, as there is no inclusions which could be observed at the subsurface crack initiation sites. Bathias and Xue [7] reported different findings from cyclic torsion fatigue test of 100Cr6 steel, and they indicated that fatigue crack initiates from subsurface inclusions of components in very high cycle regime. However, the role of inclusions on crack initiation under torsional loading in very high cycle regime has not been fully explained.

In order to evaluate the fatigue properties and resistance of the 100Cr6 steel in very high cycle regime, representative of service condition, torsion fatigue tests were conducted in this work. For the purpose of determining the fatigue strength in very high cycle regime, an ultrasonic torsion fatigue testing machine was used. To do this, four stress levels are chosen and 3–6 specimens are tested at each stress level. In addition, fracture surfaces were observed using Scanning Electronic Microscopy (SEM) in order to study the origin of fatigue crack initiation and the propagation mechanism, in relation to microstructural characteristics of the material.

## 2. Experimental aspects

### 2.1 Material

Fatigue tests were conducted with cylindrical dog-bone shaped specimens in 100Cr6 steel. The material was thermally treated with the following conditions: heating up to 850°C and kept constant during 30 minutes, then quenching at 220°C, tempering at 170° during 60 minutes. The chemical composition and the basic physical and mechanical properties of the studied 100Cr6 steel are shown in Tab. 1 and Tab. 2, respectively.

Table 1. Chemical composition of the 100Cr6 steel (wt.%)

| C | Si | Mn | P | S | Mo | Ni | Cr |
|---|---|---|---|---|---|---|---|
| 1.03 | 0.24 | 0.339 | 0.012 | 0.008 | 0.032 | 0.147 | 1.46 |

Table 2. Basic physical and mechanical properties of the 100Cr6 steel

| E/GPa | $\rho$/kg · m$^{-3}$ | $R_{e0.2\%}$/ MPa | $\sigma_b$/MPa | HV30 |
|---|---|---|---|---|
| 210 | 7870 | 1158 | 2300 | 780 |

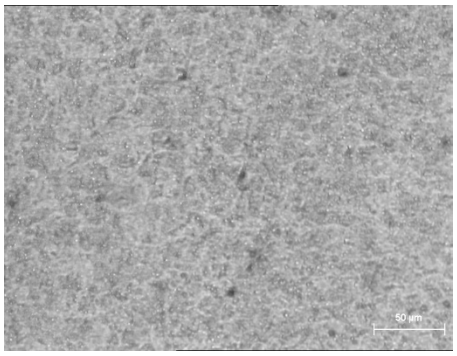


Figure 1. Optical microscopic observation of the microstructure for the 100Cr6 steel

The microstructure of the 100Cr6 steel was observed using optical microscopy, and it is shown in Fig.1. It can be seen that the ferrite and perlite phases are well distributed, and there is the presence of many large particles distributed in the material (Fig.1b).

### 2.2 Experimental procedure

In this study, fatigue tests were conducted with an ultrasonic fatigue testing machine under torsional loading, as described in [7]. Fatigue tests were carried out under constant amplitude, fully reversed loading conditions (stress ratio R=-1) at room temperature in air. In these tests, specimens are stimulated to resonance torsion vibrations, which causes fatigue loading of the specimens. The specimens were cooled with compressive air so as to reduce the temperature rise due to self-heating effect during fatigue test.

Before each test, the strain in the gage section of the specimen was calibrated using a strain gage bonded on the gage section. Under nominal elastic conditions for fatigue loading in very high cycle regime, there is a linear relationship between input displacement and the generated strain in the gage section. An example of system calibrating result is shown in Fig. 2. During fatigue tests, the test control software continuously records the displacement and controls the output of the power supplier and, therefore, indirectly controls the strain magnitude in the specimen.

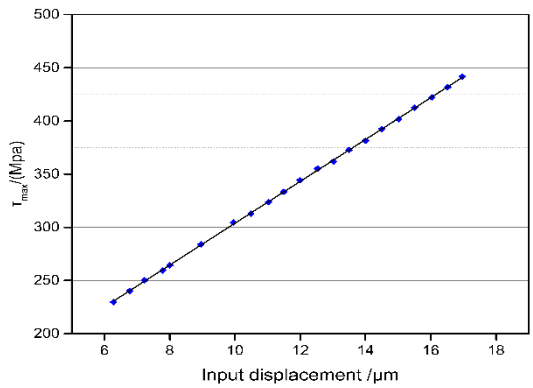


Figure 2. Example of system calibrating result showing a linear relationship between the input displacement and the generated strain in the specimen

To detect fatigue crack initiation, the vibration frequency of the system was monitored. This is because the resonance frequency of the system could be dropped with the crack initiation and propagation. Fatigue cracks could be automatically detected when the natural frequency drops a lot in a short time. The fatigue tests were stopped either when the endured number of stress cycles exceeded $10^{10}$ cycles or when the specimen was broken. After fatigue tests, the scanning electron microscope (SEM) was used to observe the fatigue cracking features on both the specimen surfaces and the fracture surfaces.

### 2.3 Fatigue specimen

Specimen dimension for torsion fatigue test was determined using analytical or numerical method. The geometry of the torsion fatigue specimen of 100Cr6 steel is shown in Fig. 3. The diameter in the centre of the specimens is 5 mm for torsional fatigue tests. All the specimens were polished up to grade 2000 paper in order to remove machining marks and to observe crack initiation and propagation path.

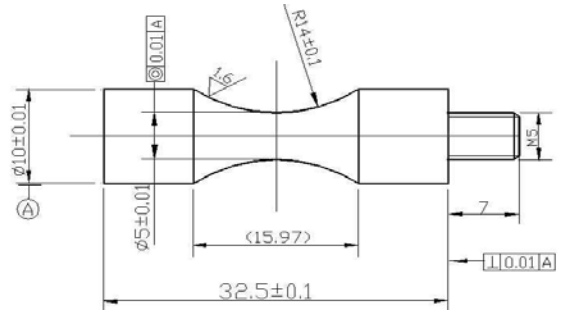


Figure 3. Dimension of 100Cr6 steel specimen tested using ultrasonic torsion fatigue testing machine

## 3. Experimental results

### 3.1 Fatigue strength

The results of the torsion fatigue experiments are presented in Fig. 4 as a plot of the torsion shear amplitude, $\tau_a$, versus the number of cycles to failure, $N_f$. Hollow circle and solid circle symbols are used for fatigue crack initiation at surface or subsurface respectively. Triangles with arrows indicate run-outs. It is important to notice that the fatigue failure occurred even beyond $10^9$ cycles for torsion fatigue tests, and there is thus no fatigue limit in very high cycle regime. According to Fig. 4, we can observe that the experimental data have relatively large dispersion at every stress level. At the stress amplitude of 620 MPa, the fatigue life ranges from $1.09 \times 10^7$ cycles to $10^{10}$ cycles.

For the specimens failed below $10^7$ cycles, there is only one specimen in which the crack initiation occurred at subsurface. However, among the 11 specimens that failed above $10^7$ cycles, 9 specimens failed due to subsurface crack initiation and 2 due to surface crack initiation, which means that ultra-high cycle fatigue life shows a clear dependency on subsurface inclusions.

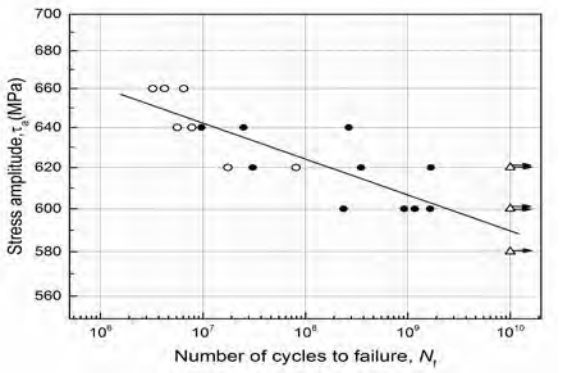


Fig.4 The S–N curves of torsion fatigue. Hollow circles indicate crack initiation at surface, while solid ones for subsurface.

In Fig. 5, the fatigue data of the material tested under axial loading presented in [7] are plotted to compare with the data tested under torsional loading. Specimens failed after $10^7$ cycles under both torsional and axial fatigue loading, and it showed larger scatter for torsional fatigue tests of the steel than axial fatigue tests. The fatigue strength at $10^9$ cycles of 100Cr6 is about 606 MPa, and the ratio between torsional and axial cyclic strength is 0.71.

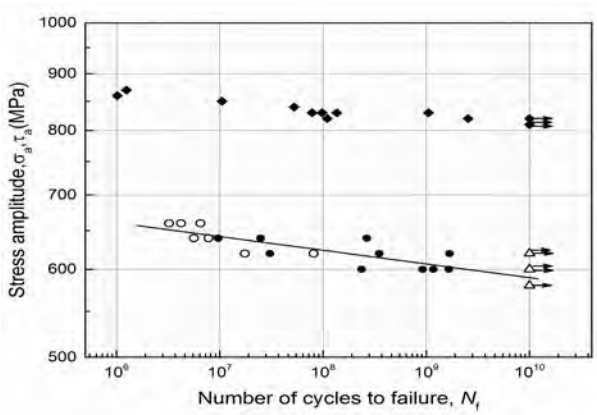


Fig.5 Comparison between the S-N curves for torsional loading (hollow and solid circles) and axial loading (solid squares)

### 3.2 Fatigue cracking mechanisms

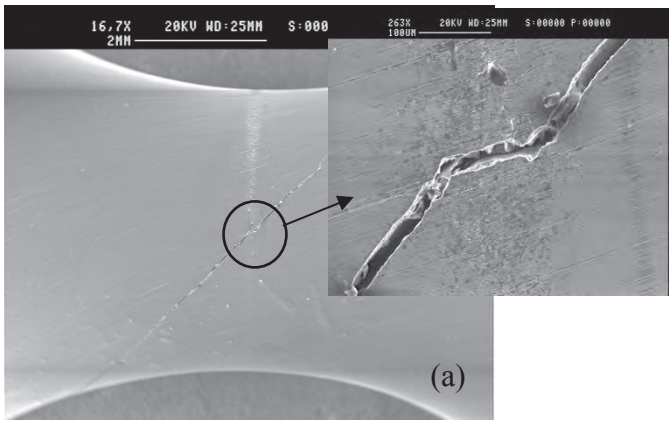


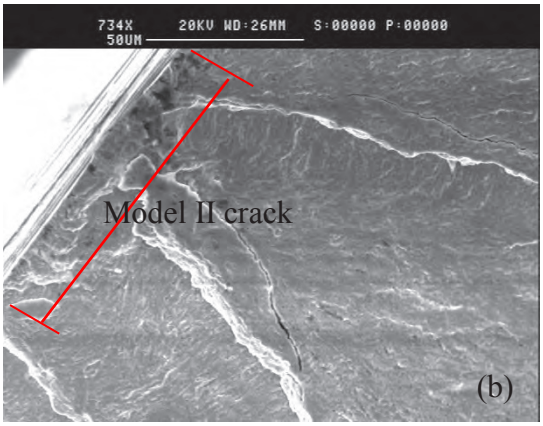

Fig. 6 Specimen surface (a) and fracture surface (b) of specimen broken after Nf = $1.75\times10^7$ under torsional loading at $\tau_a$ = 640 MPa

Both surface and subsurface crack initiation can be observed under cyclic torsional loading. Fig. 6 illustrates typical fracture surfaces for specimens with crack initiation occurring at surface. Fig. 6a shows the surface of a specimen which broke after $N_f = 1.75\times10^7$ cycles under the torsion stress amplitude $\tau_a$ = 640 MPa. The micro-crack formed during the crack initiation stage was parallel to the longitudinal direction. After the model Ⅱ crack propagated about 120 μm, it branched and propagated in a mode I manner. Fig. 6b shows the fracture surface of this specimen.

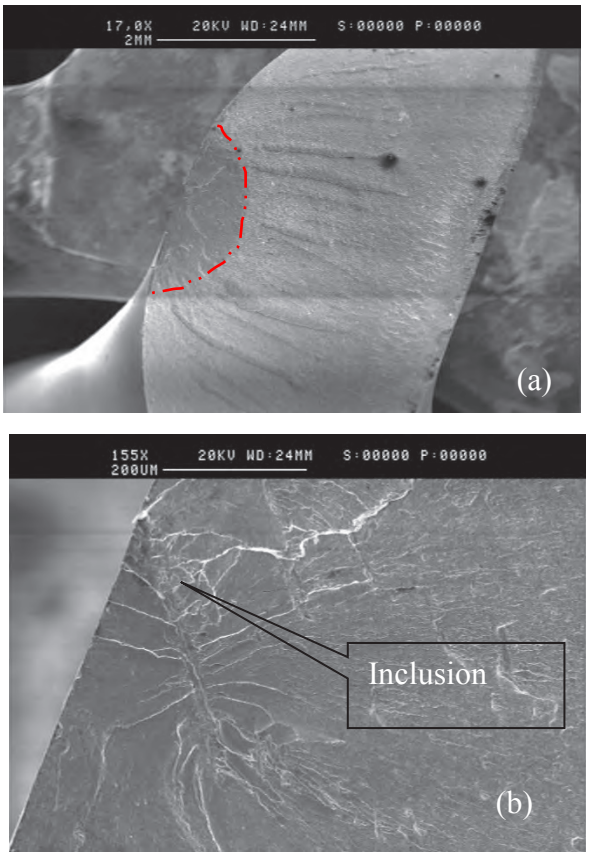


Fig.7 Fracture surface of a specimen: (a) global fatigue fracture surface with fisheye area, and (b) surface inclusion

If the fatigue fracture origin was a surface inclusion, the Mode I cracks propagated directly from the inclusion without significant Mode II growth. The macroscopic crack propagates perpendicularly to the direction of the maximum principal stress. Fig.7 shows the fracture surface of a specimen that failed after $N_f = 7.85\times10^6$ cycles at the torsion stress amplitude $\tau_a$ = 660 MPa. The surface region indicates the process of early fatigue crack growth. The first stage of crack nucleation occurs in the maximum shear plane at the tip of the inclusion, which is the maximum loaded zone under both tension and torsion loadings (Fig.7a). The surface fisheye is observed around the elongated inclusion, which presents an elliptic area with lower roughness (the area indicated by red curve in Fig.7a). A change in color from inside to outside the fisheye area can be observed. The transition from dark to light in color is related to the change of crack propagation model. Inside the fisheye, the crack propagates in hybrid model with model I and model II crack, while the Mode I crack propagation is dominant outside the fisheye area.

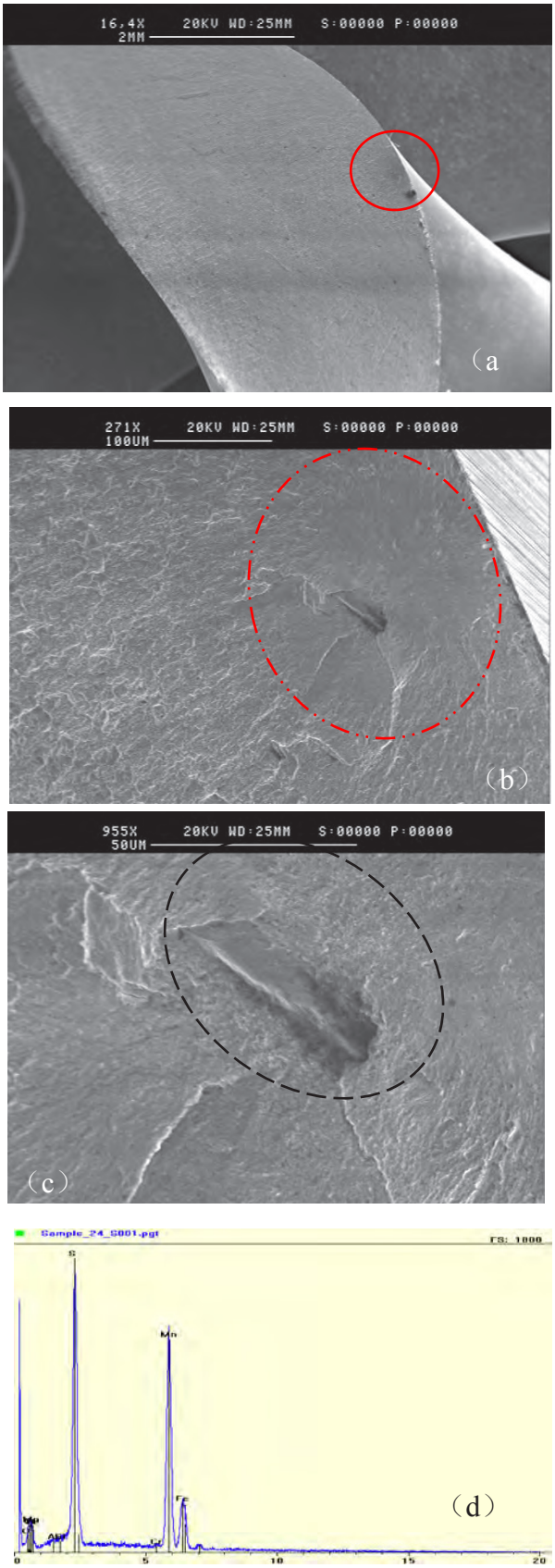

Fig.8 Fracture surface of specimen with crack initiation at subsurface: (a) global fatigue fracture surface, (b) fisheye area, and (c) FGA around inclusion, (d) chemical compositions of the inclusion analysed by EDX

Fig. 8 shows the surface and the fracture surface of a specimen that failed in the VHCF regime with a crack initiation at subsurface. A fisheye fracture surface with FGA around inclusion is visible, which was rarely reported in VHCF investigations. Fig. 8a shows stable crack propagation zone which almost covers the whole fracture surface. The fish-eye area is indicated by a red ellipse, as shown in Fig. 8b. The elliptic fish-eye area with length and width of approximately 260 μm and 210 μm respectively appears, although the boundary of the fish-eye is not very clear (see Fig. 8b). Magnification of the zone around inclusion shows that the FGA around the inclusion can be observed. The FGA area is also indicated by an ellipse in Fig. 8c, and the size of the slender inclusion inside the FGA is 54μm. The chemical composition of the inclusion on fracture surface was analyzed by Energy Dispersive Analysis of X-ray (EDX) equipped within the SEM. According to the results, this inclusion corresponds to a MnS inclusion.

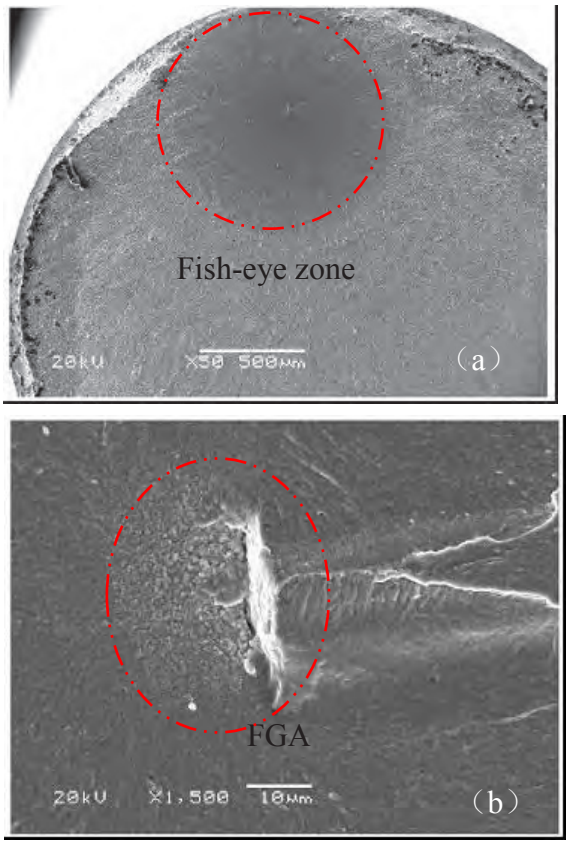


Fig. 9 Fracture surface of specimen with crack initiation at subsurface after Nf = $5.24\times10^7$ under axial loading with R = -1 at $\sigma_a$=820 MPa: (a) global fatigue fracture surface with fisheye area, and (b) FGA around inclusion

In the case of cyclic axial loading, stress distribution in the same cross section of specimen is uniform, and VHCF crack often initiates from interior inclusion for the high strength steel. Fig. 9 shows that fatigue crack initiation from a larger inclusion in VHCF regime under ultrasonic fatigue test with load ratio R = -1. It is noticed that a larger fish-eye area with clear boundary could be observed, and the inclusion is much far from the specimen surface than that in torsion fracture surface. On the other hand, unlike the spiral surface of torsion fracture surface, the crack growth under axial loading is macroscopically on the same plane.

## 4. Discussion

As presented in the literature, for high strength steels under uniaxial very high cycle fatigue loading, crack initiation often occurs at the subsurface due to the presence of metallurgical defects such as inclusions. As a matter of fact, in very high cycle regime the imposed stress amplitude is low. In this case, the macroscopic behavior of the material is in elastic regime and there is inelastic deformation only around defects such as flaws and inclusions. Since the presence probability of a defect is greater within a specimen than in its surface area, the typical crack initiation under very high cycle fatigue will be most often inside the specimen, instead of at the surface for a specimen under high cycle fatigue [7].

For a specimen subjected to torsional loading, the applied stress state is schematically presented in Fig. 10. Both the tensile and the compressive principal stresses are oriented 45° with respect to the specimen axis and they are mutually perpendicular. One shear stress component is parallel to the specimen axis, and the other is perpendicular to the specimen axis.

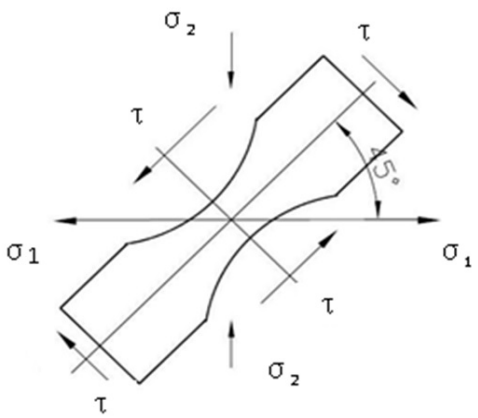


Figure 10. Schematic presentation of the stress state for a specimen under torsional loading

For all the fatigue tests conducted with a cyclic shear stress level just higher than the fatigue limit, a cracking behavior in the failed specimens has been observed. In this case, a small crack is nucleated on one of the maximum shear stress planes, and under further cyclic loading it propagated up to a length of several hundred microns. Then crack branching occurred with the increase of the number of cycles, which could generate multi-cracks. However, only one of these micro-cracks propagated following one of the planes of maximum normal stress, and lead to final fracture of specimen. Typical surface crack initiation in a specimen that failed in HCF regime (<107 cycles) is shown in Fig. 11. Crack grows in shear mode for first tens of microns, forming a

small area with steps on the fracture surface perpendicular to the specimen's length direction. The second cracks are visible on the fracture surface. After the early propagation on the planes of the maximum shear stress, the fatigue cracks could change their paths to planes perpendicular to the maximum normal stress. It means that there is always a transformation trend from model Ⅱ to model Ⅰ crack due to the effect of the normal stress, as a result, forming a spiral surface with an orientation of 45º with respect to the loading direction, as shown in Fig.12.

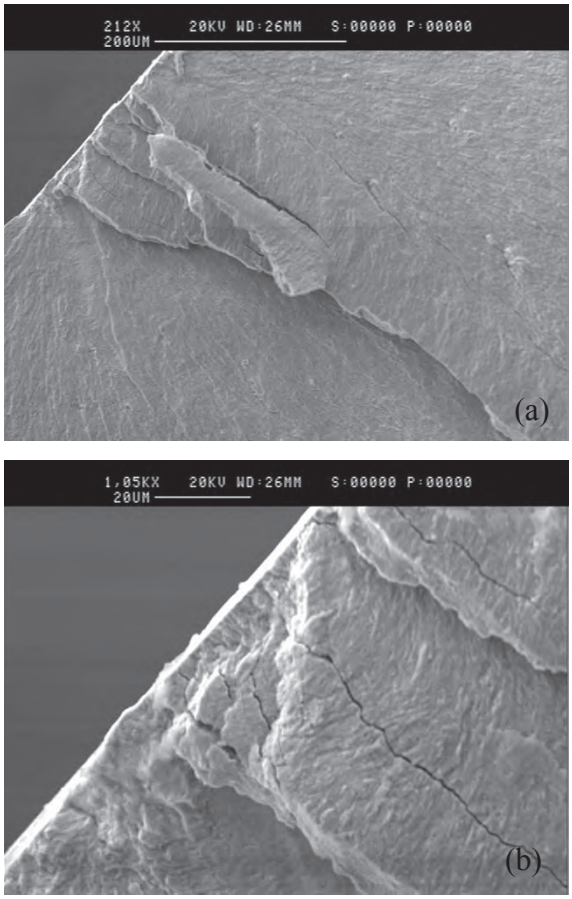


Fig. 11 Fracture surface of specimen with surface crack initiation (a), and its enlarged view (b)

Fig. 12 Spiral fracture surface of specimen under cyclic torsion loading

In VHCF regime, fatigue crack initiation started likely at subsurface of specimen. In the literature, lots of work has been done concerning the transition of fatigue crack initiation from surface to subsurface inclusion when the imposed stress amplitude is decreased [8-10]. Mechanisms for the crack initiation at subsurface inclusions have been proposed [11-13]. In general, in the case of low stress amplitude, fatigue crack initiation of most specimens is linked to the subsurface inclusion. Although macroscopically the most loaded place is on the periphery surface of specimen, the presence of an inclusion in subsurface region changes the local stress state. There is thus a competition between the stress state modification caused by inclusions and the stress on periphery surface. The stress modification at an inclusion depends on its distance from the specimen surface, and on its size and shape. It is important to note that the nature of the inclusion determines directly the crack initiation behavior. For example, a brittle inclusion may be easy to break, which leads to crack initiation. For the high strength steel investigated in the study, the maximum slender inclusion size in the critical volume of a specimen is approximately 50 μm, which is much larger than the maximum defect size of 7.9 μm characterized in [5]. Hence, for the high strength investigated in this study, most fatigue fracture occurred from subsurface defects, namely, fatigue strength was determined by the MnS inclusion in very high cycle regime.

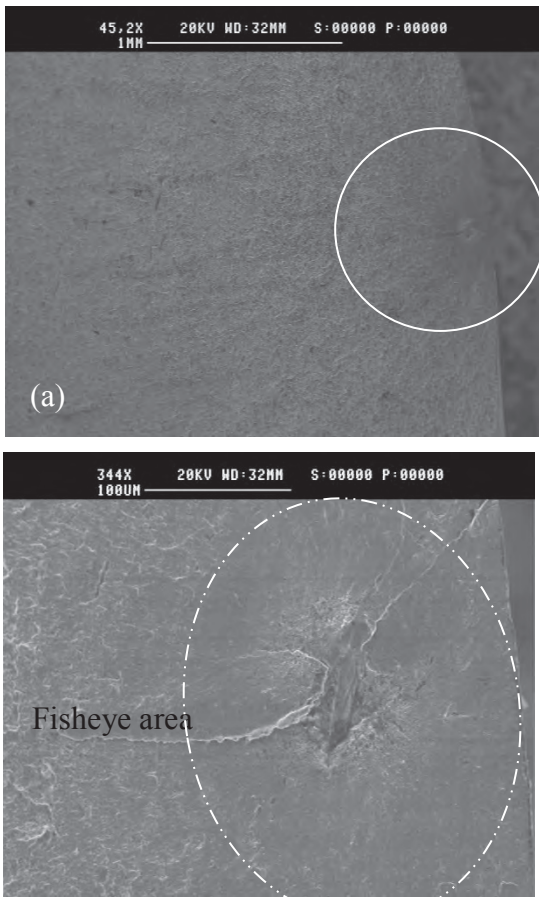

Fig.13. Illustration of an observed fracture surface showing fatigue crack initiation from the subsurface inclusion: (a) the smooth fish-eye surface, (b) enlarged view of the fish-eye area

Once a fatigue crack initiated from a subsurface inclusion, the local stress increased and complex stress states exist around the fatigue crack initiation region. Under further cyclic loading micro-crack growth took place surrounding the inclusion and progressively the cracking surface became a facet area. The surface or interior fisheye region indicates the process of early fatigue crack growth. Elliptical fish-eye area with smooth surface could be formed (Fig. 13), which is different from the stepped surface observed in [14]. Therefore, for titanium alloy in [14], crack initiation and early micro crack growth are in mode II dominated by shear loading. However, the cracks grow in mode I dominated by tensile stress in the rest of the fish eye area. For the high strength steel investigated in this study, the fish-eye fracture surface is inclined at small angle (less than 45°) perpendicular to the specimen's length axis with a successive surface. It is confirmed that the crack path inside the fish-eye is determined by both tensile and shear stress simultaneously. The difference of fisheye surface for these two kinds of materials is related to the large inclusion inside the steel. If the fatigue fracture origin was a subsurface inclusion, Mode I cracks propagated directly from the inclusion without significant Mode II growth [11]. Therefore, the facet perpendicular or parallel to the longitudinal direction due to crack initiation and early growth, could not be observed for this high strength steel in gigacycle regime.

Tensile stress on the 45° plane will exceed the tensile strength of the material before shear stress reaches the shear strength. In the very first stage of crack propagation, the fracture surface seems rather smooth. As in this stage the crack is short and of microscopic scale, the stress intensity factor is low, and the fatigue crack propagation is slow. It is important to indicate that the stage of slow crack propagation represents a large lifetime fraction of a whole fatigue test in the range of high cycle fatigue and very high cycle fatigue. When the micro-cracks reached the specimen surface, the fatigue crack propagated as surface cracks. The crack propagated along the plane loaded under cyclic tension stress, which is oriented 45° with respect to the axial direction. This orientation corresponds to the maximum principal stress plane. Although the fatigue cracking may appear to be on the maximum principal stress plane, the fatigue damage mechanism is in fact shear stress driven. As a result, the crack initiated from subsurface inclusion reveals a fracture surface oriented 45°. Thus, fatigue crack propagation occurred along the orientation normal to the 45° tensile plane, producing a spiral fracture surface. This investigation can be confirmed by Fig. 9 in which it is shown that the observation of broken specimen seems indicate that the crack propagated in 45° of axial direction.

## 5. Conclusion

In this work, torsion fatigue behavior of 100Cr6 steel in very high cycle regime was studied using an ultrasonic torsional fatigue machine. The fatigue test results indicate high scatter of obtained fatigue data due to the presence of a large number of inclusions in MnS.

Fatigue crack initiation started at the periphery surface at higher stress amplitudes. However, there is a transition of crack initiation site from surface to subsurface when the stress level was decreased and just slightly higher than very high cycle fatigue limit. Fatigue crack initiation of most specimens is linked to subsurface inclusion failure. As for the fatigue crack propagation, the fracture surface is rather smooth during the very first slow crack propagation stage. The overall crack orientation appears to follow a spiral shape on a plane with an orientation of 45º with respect to the loading direction, which corresponds to the maximum principal stress plane.

## REFERENCES

1. D. Spriestersbach, P. Grad, E. Kerscher, Procedia Engineering **74,** 84-91 (2014)
2. G.M.D. Almaraz, Mech. Mater. **40,** (2008) 636-640
3. Mayer H, J Mater Sci **44,** 4919–4929 (2009)
4. Y. Shimamura, K. Narita, H. Ishii and et al, Int. J Fatigue **60,** 57-62 (2014)
5. Y. Akiniwa, S. Stanzl-Tschegg, H. Mayer, M. Wakita, K. Tanaka, Int. J Fatigue **30,** 2057–2063 (2008)
6. H. Mayer, R. Schuller, U. Karr and et al, Int. J Fatigue **70,** 322–327 (2015)
7. H.Q. Xue, C. Bathias. Eng Fract Mech **77,** 1866–1873 (2010)
8. B. Kaiser, B. Pyttel, C. Berger. Int. J Fatigue **33,** 23–32 (2011)
9. C. Bathias, Int. J Fatigue, **23,** 143-151 (2001)
10. Nasr, Y. Nadot, Ch. Bouraoui, R. Fathallah, M. Jouiad, Int. J Fatigue 32, 780–787 (2010)
11. S. Fujita, S. Matsuoka, Y. Murakami, G. Marquis, Int. J Fatigue **32,** 943–951 (2010)
12. H. Mayer, W. Haydn, R. Schuller, S. Issler, B. Furtner, M. Bacher-Hochst, Int. J Fatigue **31,** 242-249 (2009)
13. B. Pyttel, I. Brunner, B. Kaiser, C. Berger, M. Mahendran. Int. J Fatigue **60,** 101–109 (2014)
14. A. Nikitina, T. Palin-Lucc, A. Shanyavskiy, Procedia Structural Integrity **2,** 1125–1132 (2016)